Hindawi Publishing Corporation
Journal of Chemistry
Volume 2016, Article ID 1247175, 8 pages
http://dx.doi.org/10.1155/2016/1247175

Research Article

Synthesis of Gold Nanoparticles Capped with Quaterthiophene for Transistor and Resistor Memory Devices

Mai Ha Hoang,[1] Toan Thanh Dao,[2] Nguyen Thi Thu Trang,[3] Phuong Hoai Nam Nguyen,[4] and Trinh Tung Ngo[1]

[1]*Institute of Chemistry, Vietnam Academy of Science and Technology, 18 Hoang Quoc Viet, Cau Giay, Hanoi, Vietnam*
[2]*Faculty of Electrical-Electronic Engineering, University of Transport and Communications, No. 3 Cau Giay Street, Dong Da, Hanoi, Vietnam*
[3]*Institute for Tropical Technology, Vietnam Academy of Science and Technology, 18 Hoang Quoc Viet, Cau Giay, Hanoi, Vietnam*
[4]*Faculty of Engineering Physics and Nano-Technology, University of Engineering and Technology, Vietnam National University, 144 Xuan Thuy, Cau Giay, Hanoi, Vietnam*

Correspondence should be addressed to Mai Ha Hoang; hoangmaiha@ich.vast.vn

Received 28 October 2015; Revised 4 December 2015; Accepted 24 December 2015

Academic Editor: Ahmed Mourran

Recently, the fabrication of nonvolatile memory devices based on gold nanoparticles has been intensively investigated. In this work, we report on the design and synthesis of new semiconducting quaterthiophene incorporating hexyl thiol group (**4TT**). Gold nanoparticles capped with **4TT** (**4TTG**) were prepared in a two-phase liquid-liquid system. These nanoparticles have diameters in the range 2–6 nm and are well dispersed in the poly(3-hexylthiophene) (P3HT) host matrix. The intermolecular interaction between **4TT** and P3HT could enhance the charge-transport between gold nanoparticles and P3HT. Transfer curve of transistor memory device made of **4TTG**/P3HT hybrid film exhibited significant current hysteresis, probably arising from the energy level barrier at **4TTG**/P3HT interface. Additionally, the polymer memory resistor structure with an active layer consisting of **4TTG** and P3HT displayed a remarkable electrical bistable behavior.

1. Introduction

The synthesis and characterization of gold nanoparticles have been intensively investigated because of their numerous possible applications in physics, chemistry, biology, and material science [1–3]. Recently, there have been many reports regarding the fabrication of electronic and optoelectronic devices using gold nanoparticles (AuNPs). A large number of approaches have been developed to prepare AuNPs using different ligands such as alkanethiols, phosphines, amines, and polymers [4–6]. Unfortunately, these ligands often hinder the charge transport as a dielectric layer on the surface of AuNPs. Therefore, the use of conjugated oligomers or polymers to protect AuNPs is of particular interest for the modulation of charge transfer and optical properties of these nanoparticles [7–9]. However, these AuNPs generally showed relatively poor dispersion in organic solvents that weakened their potential application in solution processing.

AuNPs have been embedded into π-conjugated host polymers to produce nanocomposites that combine the unique properties of AuNPs and π-conjugated polymers [10–15]. For solution processable fabrication, P3HT is one of the most widely used polymers because of its excellent properties [16, 17]. In this work, we prepared gold nanoparticles capped with quaterthiophene by a simple solution processing technique. These nanoparticles have a good solubility in organic solvents and are well dispersed in the host polymers. The intermolecular interaction between **4TT** and P3HT was expected to improve the charge transport between AuNP and the conjugated polymer. The presence of **4TTG** in P3HT host matrix dramatically influences the thin film transistor (TFT) memory device characteristics. We also fabricated a nonvolatile memory resistor based on P3HT and **4TTG** where P3HT serves both as matrix and active component of the device.

2. Experimental Procedure

2.1. Materials. All commercially available starting materials and solvents were purchased from Aldrich, TCI, and Acros Co. and used without further purification. All of the reactions and manipulations were carried out under N_2 with standard inertatmosphere and Schlenk techniques unless otherwise noted. Solvents used in inertatmosphere reactions were dried using standard procedures. Flash column chromatography was carried out with 230–400 mesh silica-gel from Aldrich using wet-packing method. P3HT was purchased from Sigma-Aldrich. The 2,2′-bithiophene **1**, 5-dodecyl-2,2′-bithiophene **4**, and 2-(5′-dodecyl-2,2′-bithiophen-5-yl)-4,4,5,5-tetramethyl-1,3,2-dioxaborolane **5** were prepared according to the modified literature procedures [18].

2.2. Synthesis

*5-(6-Bromohexyl)-2,2′-bithiophene **2***. A solution of bithiophene **1** (24.9 g, 0.15 mol) in 300 mL tetrahydrofuran (THF) was cooled to −78°C in an acetone/dry ice bath. N-Butyllithium (0.16 mol, 64 mL, 2.5 M in hexane) was added through a syringe over 10 min. The temperature of the reaction mixture was slowly raised to −30°C and was maintained for 1 h. After that, the reaction mixture was cooled again to −78°C, and 1,6-dibromohexane (146.4 g) was added via syringe. The mixture was stirred for 30 min at −78°C and the bath was then removed, the solution was stirred for an additional 3 h while the temperature was increased slowly to room temperature. The reaction mixture was next poured into 500 mL of dichloromethane (DCM) and 200 mL of 1 M NH_4Cl solution. The organic phase was separated, washed with water, dried over sodium sulfate, and concentrated. The residue was crystallized with methanol to remove 1,6-dibromohexane. The resultant precipitate was purified with silica-gel column chromatography using chloroform/hexane (1/50 v/v) and then crystallized in methanol to afford 25.6 g of solid: yield 52%.

^{1}H-NMR (300 MHz, $CDCl_3$). δ(ppm) 7.16 (dd, J_1 = 5.2 Hz, J_2 = 1.6 Hz, 1H), 7.09 (dd, J_1 = 4.0 Hz, J_2 = 1.6 Hz, 1H), 6.98 (d, J = 4.0 Hz, 1H), 6.94 (d, J = 4.0 Hz, 1H), 6.67 (d, J = 4.0 Hz, 1H), 3.42 (t, 2H), 2.79 (t, 2H), 1.86 (m, 2H), 1.69 (m, 2H), 1.37–1.51 (m, 4H).

*5-Bromo-5′-(6-bromohexyl)-2,2′-bithiophene **3***. A solution of 5-(6-bromohexyl)-2,2′-bithiophene **2** (9.2 g, 28 mmol) in 150 mL DCM was cooled to 0°C. N-Bromosuccinimide (NBS, 5.3 g, 30 mmol) was added. The mixture was stirred at room temperature overnight. Then, 200 mL water was added to the reaction mixture. The organic phase was separated, washed with water, dried over sodium sulfate, and concentrated. The residue was purified with silica-gel column chromatography using hexane to afford 9.43 g of colorless oil: yield 83%.

^{1}H-NMR (300 MHz, $CDCl_3$). δ(ppm) 6.94 (d, J = 4.0 Hz, 1H), 6.91 (d, J = 4.0 Hz, 1H), 6.83 (d, J = 4.0 Hz, 1H), 6.67 (d, J = 4.0 Hz, 1H), 3.41 (t, 2H), 2.79 (t, 2H), 1.87 (m, 2H), 1.69 (m, 2H), 1.37–1.51 (m, 4H).

*5-Dodecyl-5′-(6-bromohexyl)-2,2′-quaterthiophene **6***. 5-Bromo-5′-(6-bromohexyl)-2,2′-bithiophene **3** (3.22 g, 7 mmol), 2-(5′-dodecyl-2,2′-bithiophen-5-yl)-4,4,5,5-tetramethyl-1,3,2-dioxaborolane **5** (2.84 g, 7 mmol), and tetrakis (triphenylphosphine) palladium (230 mg, 0.2 mmol) were dissolved in 50 mL of toluene under an argon atmosphere. The resultant mixture was stirred at room temperature for 5 min before an aqueous K_2CO_3 solution (15 mL, 2 M) was added. The mixture was stirred for 24 h at 90°C under nitrogen. Then, the mixture was cooled down to room temperature and neutralized with 1 M HCl solution. The organic layer was separated and the aqueous phase was extracted with DCM. The combined organic layer was condensed and the residue was purified with silica-gel column chromatography using chloroform/hexane (1/5 v/v) to afford 3.01 g of yellow solid: yield 65%.

^{1}H-NMR (300 MHz, $CDCl_3$). δ(ppm) 7.04 (d, J = 4.0 Hz, 2H), 6.99 (d, J = 4.0 Hz, 2H), 6.97 (d, J = 4.0 Hz, 2H), 6.69 (m, 2H), 3.42 (t, 2H), 2.76–2.83 (m, 4H), 1.85–1.90 (m, 2H), 1.65–1.73 (m, 4H), 1.26–1.47 (m, 22H), 0.88 (t, 3H).

Anal. Calcd. for $C_{34}H_{45}BrS_4$. C, 61.70; H, 6.85; Br, 12.07; S, 19.38 Found: C, 61.78; H, 6.75; Br, 12.09; S, 19.35. MS (MALDI-TOF) m/z $[M]^+$: Calcd. for $C_{34}H_{45}BrS_4$, 661.89; found 662.1

*5-Dodecyl-5′-(6-ethanethioatehexyl)-2,2′-quaterthiophene **7***. A solution of 5-dodecyl-5′-(6-bromohexyl)-2,2′-quaterthiophene **6** (1.99 g, 3 mmol) and potassium thioacetate (0.68 g, 6 mmol) in 100 mL N,N-dimethylformamide was stirred at 90°C overnight. Then, the mixture was cooled down to room temperature and 100 mL water was added to the reaction mixture. The resultant precipitate was filtered and washed with methanol and then purified with silica-gel column chromatography using chloroform/hexane (1/1 v/v). After that, it was crystallized in THF/methanol to afford 1.71 g of yellow solid: yield 87%.

^{1}H-NMR (300 MHz, $CDCl_3$). δ(ppm) 7.03 (d, J = 4.0 Hz, 2H), 6.99 (d, J = 4.0 Hz, 2H), 6.97 (d, J = 4.0 Hz, 2H), 6.68 (m, 2H), 2.87 (t, 2H), 2.79 (t, 4H), 2.33 (s, 3H), 1.66–1.70 (m, 6H), 1.26–1.42 (m, 22H), 0.88 (t, 3H).

Anal. Calcd. for $C_{36}H_{48}OS_5$. C, 65.80; H, 7.36; O, 2.43; S, 24.40 Found: C, 65.77; H, 7.42; S, 24.32. MS (MALDI-TOF) m/z $[M]^+$: Calcd. for $C_{36}H_{48}OS_5$, 657.09; found 657.20.

*5-Dodecyl-5′-(6-thiolhexyl)-2,2′-quaterthiophene **4TT***. 5-Dodecyl-5′-(6-ethanethioatehexyl)-2,2′-quaterthiophene **7** (1.51 g, 2.3 mmol) was dissolved in 100 mL THF. A solution of potassium hydroxide (0.28 g, 5 mmol) in 5 mL ethanol was added and the mixture was stirred at room temperature overnight. Then, 200 mL of water was added slowly to precipitate out the product. The resultant precipitate was

filtered and washed with methanol and then purified with silica-gel column chromatography using chloroform. After that, it was crystallized in DCM/methanol to afford 1.3 g of yellow solid: yield 92%.

^{1}H-NMR (300 MHz, $CDCl_3$). δ(ppm) 7.03 (d, J = 4.0 Hz, 2H), 6.99 (d, J = 4.0 Hz, 2H), 6.97 (d, J = 4.0 Hz, 2H), 6.68 (m, 2H), 2.77–2.81 (m, 4H), 2.50–2.56 (m, 2H), 1.61–1.71 (m, 6H), 1.26–1.44 (m, 22H), 0.88 (t, 3H).

^{13}C-NMR (100 MHz, $CDCl_3$). δ(ppm) 145.67, 145.25, 136.72, 136.59, 135.37, 135.27, 134.53, 134.40, 124.92, 124.83, 124.00, 123.59, 123.35, 33.88, 31.92, 31.59, 31.41, 30.19, 30.07, 29.64, 29.36, 29.07, 28.45, 28.05, 24.60, 22.70, 14.15.

Anal. Calcd. for $C_{34}H_{46}S_5$. C, 66.39; H, 7.54; S, 26.07 Found: C, 66.35; H, 7.42; S, 26.18. MS (MALDI-TOF) m/z $[M]^+$: Calcd. for $C_{34}H_{46}S_5$, 615.05; found 615.20.

*Synthesis of Gold Nanoparticles Capped with Quaterthiophene **4TTG***. An aqueous solution of hydrogen tetrachloroaurate (60 mL, 0.015 M) was mixed with a solution of tetraoctylammonium bromide in toluene (80 mL, 0.05 M). The two-phase mixture was vigorously stirred until all the tetrachloroaurate was transferred into the organic layer and the color changed to orange. **4TT** (0.18 g, 0.3 mmol) in 60 mL toluene was then added to the organic phase. The mixture was stirred at 70°C for 1 h. Then, the mixture was cooled down to room temperature and an aqueous solution of sodium borohydride (50 mL, 0.2 M) was slowly added with vigorous stirring. After further stirring for 6 h the organic phase was separated, washed with water, dried over sodium sulfate, and concentrated. Finally, **4TTG** was precipitated in DCM/acetonitrile to afford 0.3 g of dark brown solid.

^{1}H-NMR (300 MHz, $CDCl_3$). δ(ppm) 7.03 (d, J = 4.0 Hz, 2H), 6.99 (d, J = 4.0 Hz, 2H), 6.96 (d, J = 4.0 Hz, 2H), 6.68 (m, 2H), 3.25–3.31 (m, 2H), 2.77–2.81 (m, 4H), 1.60–1.65 (m, 6H), 1.26–1.42 (m, 22H), 0.88 (t, 3H).

Elemental Analysis. Au, 64.02%; C, 23.78%; H, 2.61%; S, 9.59%.

2.3. Instrumentation. ^{1}H NMR spectra were recorded on a Varian AS400 (399.937 MHz for 1H and 100.573 MHz for 13C) spectrometer. ^{1}H chemical shifts are referenced to the proton resonance resulting from protic residue in deuterated solvent and ^{13}C chemical shift recorded downfield in ppm relative to the carbon resonance of the deuterated solvents. MALDI-TOF analysis was performed on a Voyager-DE STR MALDI-TOF mass spectrometer. The elemental analyses for measuring the composition of C, H, S, and N were performed on an EA1112 (Thermo Electron Corp., West Chester, PA, USA) elemental analyzer. Thermal properties were studied on a TGA50 (Heating rate of 5°C/min). All transmission electron microscopy (TEM) images were obtained at 200 keV with LaB6 filament, using a Tecnai G2 F20 S-Twin and recorded with a 2 K × 2 K pixel resolution Veleta TEM camera (Olympus) on Cu TEM grids. Absorption and emission spectra were obtained using an HP-8453 spectrophotometer (photodiode array type) and Hitachi F-7000 fluorescence spectrophotometer using quartz cells, respectively. The redox properties of **4TT** and P3HT molecules were examined using cyclic voltammetry (CV, EA161 eDAQ). The electrolyte solution employed was 0.10 M tetrabutylammonium hexafluorophosphate (Bu_4NPF_6) in a freshly dried MC. The Ag/AgCl and Pt wire (0.5 mm in diameter) electrodes were used as the reference and counter electrode, respectively. The scan rate was 50 mV/s. Atomic Force Microscopy (AFM, Advanced Scanning Probe Microscope, XE-100, PSIA) operating in the tapping mode with a silicon cantilever (type A, resonant frequency: 150 kHz) was used to characterize the surface morphologies of the thin film samples.

2.4. TFT Memory Fabrication. To study charge transport properties of the **4TTG**/P3HT blend, bottom-gate/top-contact (BGTC) TFT device structure was employed. The gate electrode was n-type doped ⟨100⟩ silicon wafer and the SiO_2 gate insulator has a thickness of 300 nm. The substrate was cleaned thoroughly by a series of ultrasonications in different solvents such as acetone, cleaning agent, deionized water, and isopropanol. The cleaned substrates were dried under vacuum at 120°C for 1 h and then treated with UV/ozone for 20 min. Then, the wafers were immersed in a 8 mmol/L solution of n-octyltrichlorosilane (OTS) in anhydrous toluene for 30 min to generate a hydrophobic insulator surface. The active layer (**4TTG**/P3HT: 1/9) was deposited on the OTS-treated substrates by spin-coating polymer solutions (1%) at 1500 rpm for 40 s. Finally, the source and drain electrodes were prepared using thermal evaporation of gold (100 nm) through a shadow mask with a channel width of 1500 μm and a channel length of 100 μm. Transfer characteristics of the devices were determined in air using a Keithley 4200 SCS semiconductor parameter analyzer.

2.5. Resistor Memory Device Fabrication. The memory devices were fabricated according to the modified literature procedures [15, 17]. The first step involved preparation of the substrate. Glass substrates were cleaned with detergent, deionized water, acetone, and isopropyl alcohol in an ultrasonic bath. The substrates were dried for 2 h and subsequently treated with UV ozone for 20 min. After that, the bottom aluminum (Al) electrode was deposited by using a thermal evaporator with a shadow metal mask at a base pressure of 2×10^{-6} torr. The UV-ozone treatment was repeated again to activate the Al surface. The active layer of 50 nm was formed by spin coating a solution of 0.9 wt% P3HT and 0.1 wt% **4TTG**. Finally, the top Al electrode was deposited. Both the electrodes have a thickness of 70 nm. The device had an area of 2 × 2 mm^2. The electrical characteristics of the device were also measured using Keithley 4200-SCS semiconductor characterization system under ambient conditions.

3. Results and Discussions

3.1. Synthesis. We report the easy, high-yield synthesis of new semiconducting quaterthiophene **4TT** incorporating hexyl

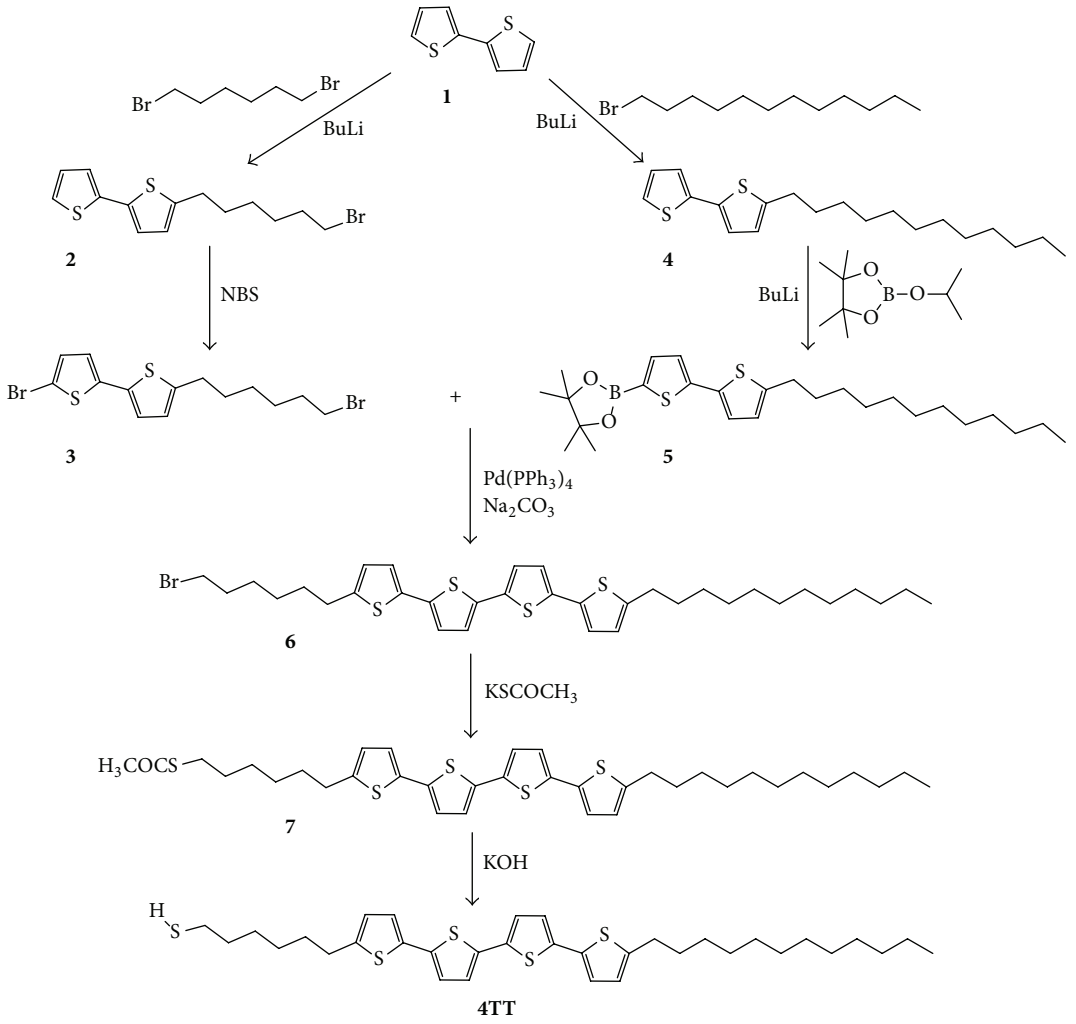

Scheme 1: Synthetic route of **4TT**.

thiol group. In comparison with reported quaterthiophene analogues [19–22], this compound bears two long alkyl chains that could improve its solubility. In Scheme 1, the Suzuki coupling reaction of 5-bromo-5′-(6-bromohexyl)-2,2′-bithiophene **3** and 2-(5′-dodecyl-2,2′-bithiophen-5-yl)-4,4,5,5-tetramethyl-1,3,2-dioxaborolane **5** was conducted in the presence of a catalytic amount of tetrakis(triphenylphosphine) palladium to afford compound **6**. This compound was converted to compound **7**. After removing the ethanethioate group, **4TT** was obtained in good yield.

We prepared gold nanoparticles **4TTG** by keeping the concentration of hydrogen tetrachloroaurate, tetraoctylammonium bromide and varying the concentration of the ligand **4TT** (Figure 1(a)). It was found that the mole ratio of 3/1 (Au/**4TT**) was optimum for the formation of AuNPs capped with **4TT** without the aggregation of nanoparticles.

The NMR of **4TTG** and **4TT** was similar, which indicated that AuNPs were capped with **4TT**. Elemental analysis gave the following: Au, 64.02%; C, 23.78%; H, 2.61%; S, 9.59%. The C : H : S ratios of **4TTG** and **4TT** were similar further confirming the formation of **4TT** layer on the AuNPs. Thermogravimetric analysis (TGA) showed that the **4TTG** started losing mass at about 265°C. The weight loss from room temperature to 800°C was about 35% that well matched the elemental analysis result.

3.2. Morphology of QTTG. TEM images of the **4TTG** (Figure 1(b)) showed that they were narrow polydispersed nanoparticles with diameters in the range 2–6 nm. The narrow polydispersity of AuNPs could result from the formation of a self-assembled **4TT** layer on the growing nuclei. In comparison with dodecanethiol-protected AuNPs, the particles size of **4TTG** was bigger. It is because of the steric effect that restricted the interaction between **4TT** and the surface of AuNPs.

3.3. Optical and Electrochemical Properties. The solution samples were prepared in chloroform with a concentration of 1×10^{-6} M, and the thin film samples were fabricated

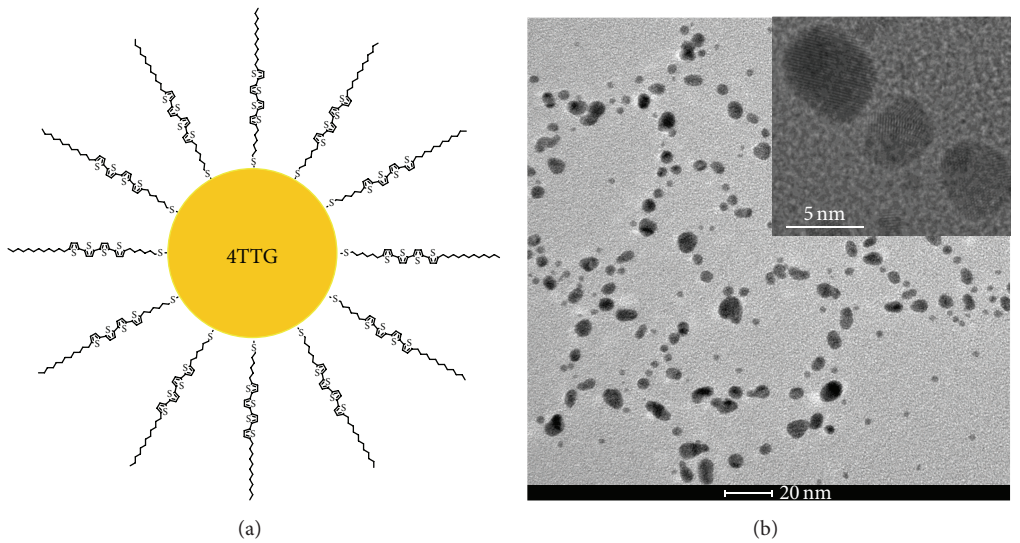

Figure 1: Schematic illustration of self-assembled **4TT** layer on the AuNPs (a) and TEM images of **4TTG** (b).

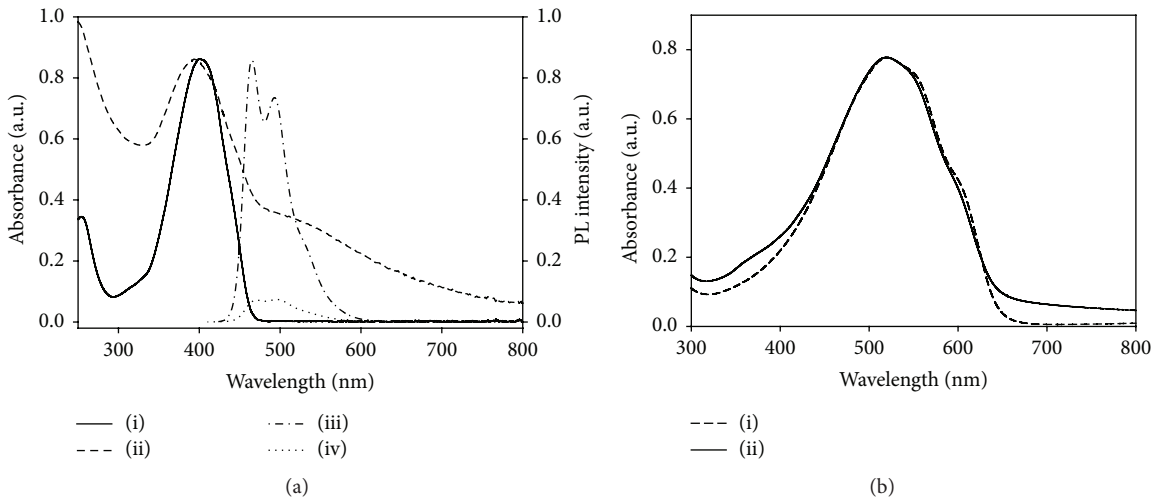

Figure 2: UV-vis absorption and PL emission spectra. (a) UV-vis absorption spectra of **4TT** (i) and **4TTG** (ii), PL emission spectra of **4TT** (iii) and **4TTG** (iv) in solution state; (b) UV-vis absorption spectra of P3HT (i) and a composite of 10% **4TTG** in P3HT (ii) in film state.

by spin-coating with 1 wt% solutions. The absorption spectra of **4TT** and **4TTG** in solution state were shown in Figure 2(a). **4TT** showed an absorption maximum at 401 nm while **4TTG** exhibited an absorption maximum at 395 and a shoulder at 500–550 nm; those were contributed by **4TT** and AuNPs, respectively. This spectrum suggested that the average particle size of **4TTG** was below 5 nm because larger particles often exhibit a sharper and more intense plasmon absorption band close to 525 nm [4]. **4TT** exhibited PL spectral behavior with emission maxima at 466 and 493 nm in solution state. Interestingly, the PL spectrum of **4TTG** showed low efficiency due to their self-absorption.

The absorption spectra of P3HT and the composite of 10% **4TTG** in P3HT in film state were shown in Figure 2(b). Similar absorption maxima of these films were located at 520 nm. A slight float was observed in the film state of the composite, which was attributed to the presence of **4TTG** in the matrix. The composite also showed a good film forming that could be used for the device fabrication.

CV measurements were taken to determine the oxidation potentials of **4TT** and P3HT. We combined the oxidation potential in CV with the optical energy band gap (E_g^{opt}) as determined by the cut-off absorption wavelength in the absorption spectrum to calculate the lowest unoccupied molecular orbital (LUMO) levels. **4TT** and P3HT were found to have the highest occupied molecular orbital (HOMO) levels of −5.18 and −5.02 eV, respectively. Concomitantly, **4TT** and P3HT have LUMO energy levels of −2.52 and −3.12 eV, respectively.

3.4. Atomic Force Microscopic Study. AFM images of P3HT and the nanocomposite of 10% **4TTG** in P3HT were shown in

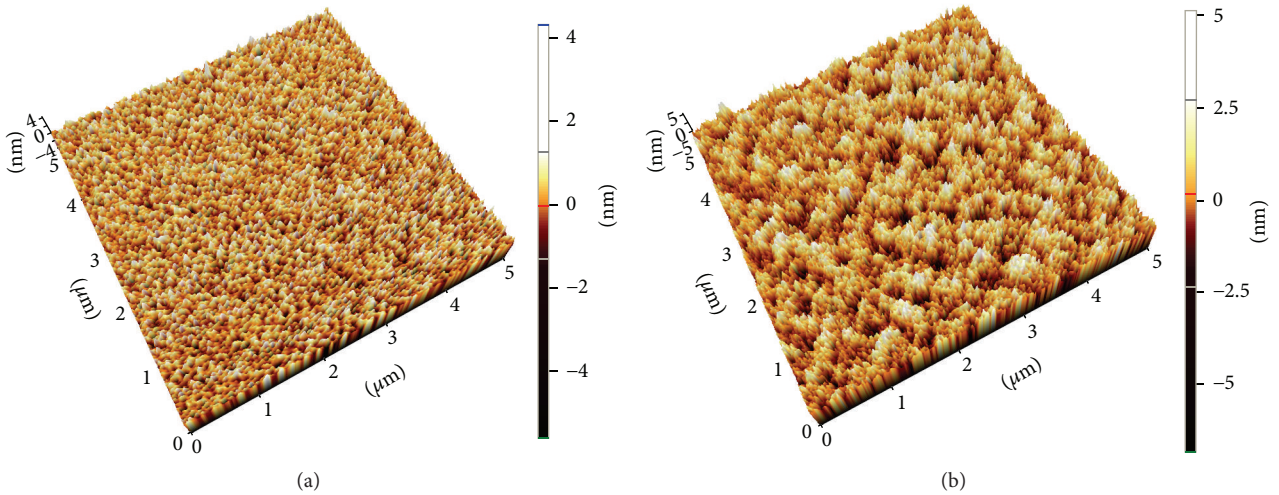

Figure 3: AFM topographic images ($5 \times 5\,\mu$m) of the spin-coated films of P3HT (a) and **4TTG**/P3HT (b).

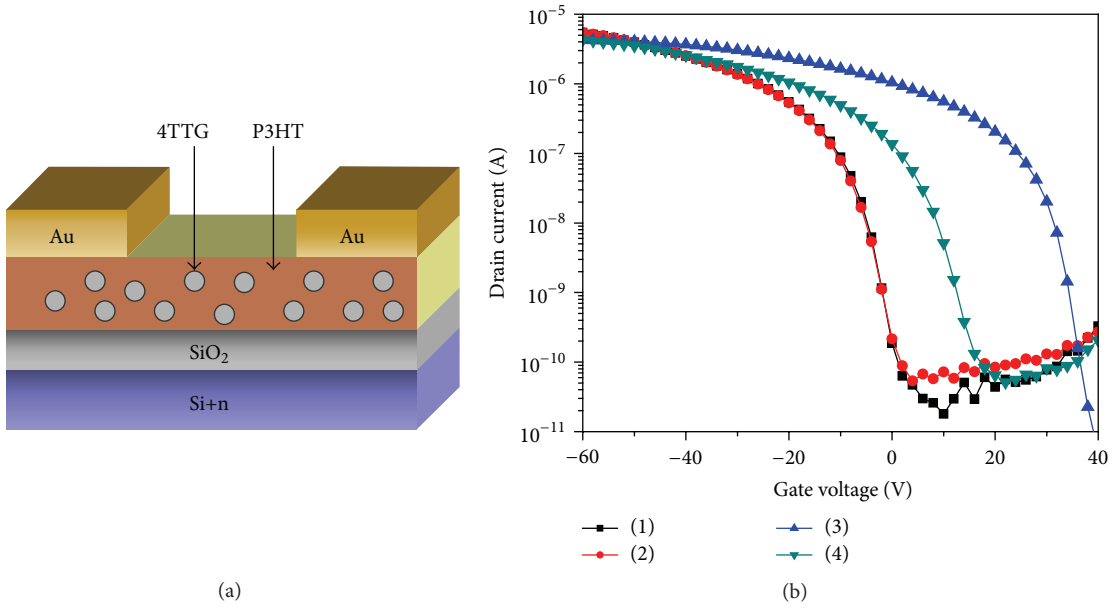

Figure 4: (a) TFT device structure using **4TTG**/P3HT as active layer and (b) transfer characteristics of the Au/P3HT/Au (programed (curve (1)) and erased (curve (2)) states) and Au/**4TTG** + P3HT/Au (programed (curve (3)) and erased (curve (4)) states) devices.

Figure 3. P3HT and the blend of **4TTG**/P3HT were dissolved in chloroform and the resulting solutions were then spin-coated on silicon wafers. The surface morphology of P3HT and the blend of **4TTG**/P3HT thin films exhibited root mean squares (RMS) roughness values of 0.9 and 1.2 nm, respectively. The topography of **4TTG**/P3HT thin films showed small surface roughness that indicated a high miscibility of **4TTG** on the hybrid film.

3.5. TFT Memory Characteristics. Figure 4(b) exhibited the transfer curves of TFT devices with and without **4TTG** upon double sweeping where the cyclic sweeping of the gate voltage was operated from 40 V to −60 V and then back to 40 V. These TFT devices showed the p-type characteristics. Transfer curve of neat P3HT film displayed no hysteresis with near-zero threshold voltage (V_{th}). By contrast, transfer curve of **4TTG**/P3HT hybrid film exhibited significant current hysteresis, probably arising from the charge trapping effect of the **4TTG** in the P3HT matrix [10, 13]. The memory window (ΔV_{th}), defined as the change in V_{th} between programmed and erased characteristics, was estimated to be around 20 V. Indeed, charge trapping/detrapping by AuNPs would modulate the conductivity of the P3HT transistor channel, resulting in a change in the transfer curves.

3.6. Resistor Memory Behavior. Figure 5(a) shows the resistive device structure with a polymer layer sandwiched between two aluminum electrodes. The active layer consists

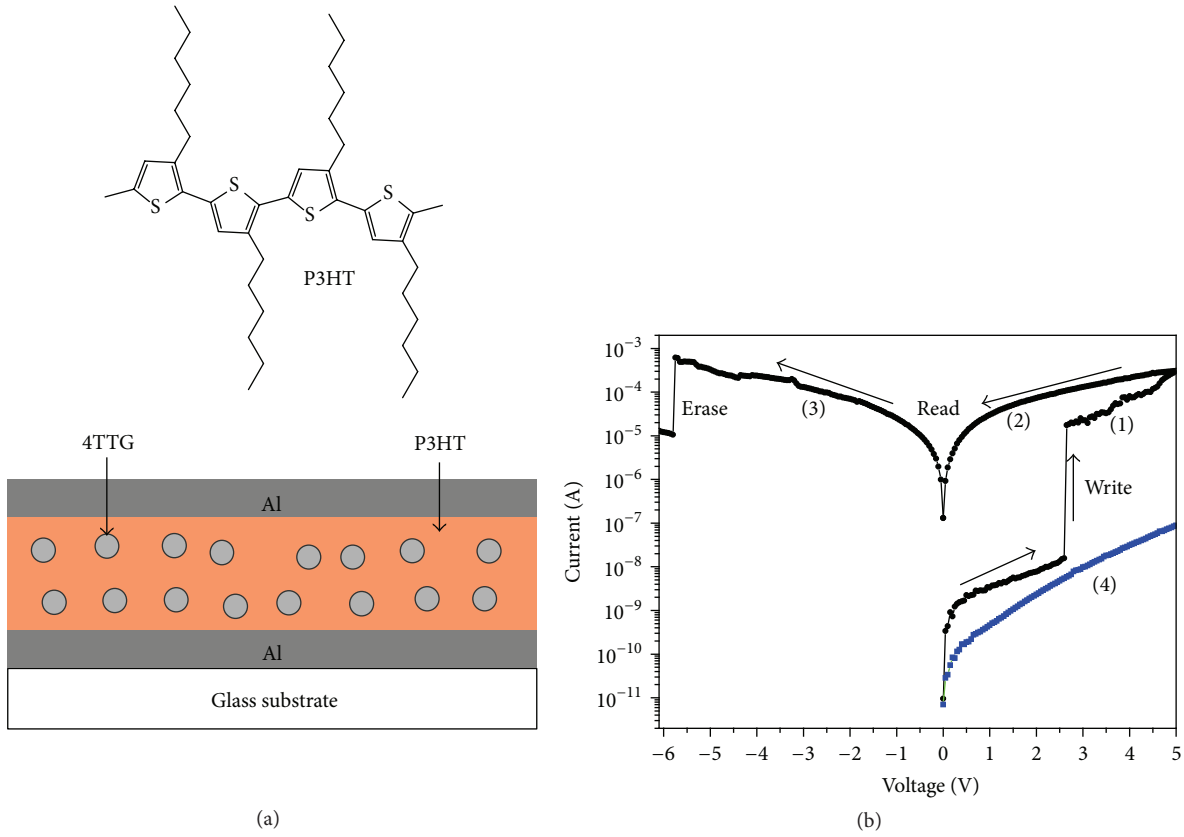

Figure 5: (a) Device structure and (b) current-voltage (I-V) characteristics of the Al/**4TTG** + P3HT/Al and Al/P3HT/Al resistor memory devices. Curves (1), (2), and (3) represent the first, second, and third bias scans of the Al/**4TTG** + P3HT/Al device. Curve (4) is the I-V curve of the Al/P3HT/Al device.

of a P3HT film containing 10% **4TTG** nanoparticles. **4TTG** were selected in this device because gold nanoparticles were capped with quaterthiophene thiol. The quaterthiophene has a similar structure with P3HT that might lead to an effective intermolecular interaction and charge transfer between **4TTG** and P3HT.

Figure 5(b) shows the current-voltage (I-V) curve of the device. Two distinct conducting states were observed. The pristine device showed a low current when the applied voltage was from 0 to 2.5 V, which corresponds to the "0" state of a bistable memory [15, 17]. When the applied voltage was approaching 2.7 V, a remarkably abrupt current increase from 2×10^{-8} to 4×10^{-5} A was observed (curve (1)). The device still remained in the high-conductivity state (on-state) in the subsequent scan (curve (2)). The on/off current ratio at 1 V was obtained to be more than four orders of magnitude. After the large applied voltage was removed, the on-state still remained, which corresponded to the "1" state of a memory. This phenomenon demonstrated a nonvolatile memory behavior. When the applied voltage was reaching −5.7 V, a high-conductivity state returned to the low-conductivity as shown in curve (3). After the device was restored to its low-conductivity state, once again, it could exhibit a similar I-V characteristic as in the first voltage sweep, which indicated that the device has a rewritable nonvolatile property. On the other hand, the device that used a pure P3HT without **4TTG** in the active layer did not exhibit a significant current hysteresis (curve (4)). In this device, the I-V curve still showed a low-conductivity state even when the applied voltage went as high as 7 V. For comparison, the memory device that used P3HT and dodecanethiol-protected AuNPs showed an ambiguous current jump in off-state and unclear erase behavior [17]. This phenomenon could be explained by the role of quaterthiophene layer of **4TTG**. Quaterthiophene group can interact with P3HT and thereby enhances the charge-transport between **4TTG** and P3HT.

4. Conclusion

In conclusion, gold nanoparticles capped with quaterthiophene were successfully prepared in a two-phase liquid-liquid system. These particles have diameters in the range 2–6 nm and are well dispersed in organic solvents. The intermolecular interaction between **4TT** and P3HT could enhance the charge-transport between gold nanoparticles and the host polymer. Transfer curve of TFT device made of **4TTG**/P3HT hybrid film exhibited significant current hysteresis. A polymer memory device using P3HT and **4TTG** exhibited a repeatable bistable behavior and high stability even after a large number of read-write-erase cycles. Four

orders of magnitude difference between the on and off currents was achieved. This report contributes to the preparation of gold nanoparticles for the nonvolatile electronic memory.

Conflict of Interests

The authors declare that there is no conflict of interests regarding the publication of this paper.

Acknowledgments

This research is funded by Vietnam National Foundation for Science and Technology Development (NAFOSTED) under Grant no. "104.02-2013.67". The authors acknowledge Professor Dong Hoon Choi (Korea University) for his kind support.

References

[1] B. Zhang, T. Cai, S. Li et al., "Yolk-shell nanorattles encapsulating a movable Au nanocore in electroactive polyaniline shells for flexible memory device," *Journal of Materials Chemistry C*, vol. 2, no. 26, pp. 5189–5197, 2014.

[2] P. Kannan and S. Abraham John, "Synthesis of mercaptothiadiazole-functionalized gold nanoparticles and their self-assembly on Au substrates," *Nanotechnology*, vol. 19, no. 8, Article ID 085602, 2008.

[3] E. Boisselier, L. Salmon, J. Ruiz, and D. Astruc, "How to very efficiently functionalize gold nanoparticles by 'click' chemistry," *Chemical Communications*, no. 44, pp. 5788–5790, 2008.

[4] I. Hussain, S. Graham, Z. Wang et al., "Size-controlled synthesis of near-monodisperse gold nanoparticles in the 1–4 nm range using polymeric stabilizers," *Journal of the American Chemical Society*, vol. 127, no. 47, pp. 16398–16399, 2005.

[5] M. Brust, M. Walker, D. Bethell, D. J. Schiffrin, and R. Whyman, "Synthesis of thiol-derivatised gold nanoparticles in a two-phase liquid-liquid system," *Journal of the Chemical Society, Chemical Communications*, no. 7, pp. 801–802, 1994.

[6] X. Xu, N. L. Rosi, Y. Wang, F. Huo, and C. A. Mirkin, "Asymmetric functionalization of gold nanoparticles with oligonucleotides," *Journal of the American Chemical Society*, vol. 128, no. 29, pp. 9286–9287, 2006.

[7] B. Vercelli, G. Zotti, and A. Berlin, "Star-shaped and linear terthiophene-thiol self-assembled monolayers as scaffolds for gold nanoparticles," *Chemistry of Materials*, vol. 19, no. 3, pp. 443–452, 2007.

[8] B. Vercelli, G. Zotti, and A. Berlin, "Gold nanoparticles linked by pyrrole- and thiophene-based thiols. Electrochemical, optical, and conductive properties," *Chemistry of Materials*, vol. 20, no. 2, pp. 397–412, 2008.

[9] T. Kudernac, S. J. Molen, B. J. Wees, and B. L. Feringa, "Uni- and bi-directional light-induced switching of diarylethenes on gold nanoparticles," *Chemical Communications*, pp. 3597–3599, 2006.

[10] H.-C. Chang, C.-L. Liu, and W.-C. Chen, "Nonvolatile organic thin film transistor memory devices based on hybrid nanocomposites of semiconducting polymers: gold nanoparticles," *ACS Applied Materials and Interfaces*, vol. 5, no. 24, pp. 13180–13187, 2013.

[11] V. Suresh, D. Y. Kusuma, P. S. Lee, F. L. Yap, M. P. Srinivasan, and S. Krishnamoorthy, "Hierarchically built gold nanoparticle supercluster arrays as charge storage centers for enhancing the performance of flash memory devices," *ACS Applied Materials and Interfaces*, vol. 7, no. 1, pp. 279–286, 2015.

[12] L. Marino, S. Marino, D. Wang, E. Bruno, and N. Scaramuzza, "Nonvolatile memory effects in an orthoconic smectic liquid crystal mixture doped with polymer-capped gold nanoparticles," *Soft Matter*, vol. 10, no. 21, pp. 3842–3849, 2014.

[13] Y. Zhou, S.-T. Han, Z.-X. Xu, and V. A. L. Roy, "Low voltage flexible nonvolatile memory with gold nanoparticles embedded in poly(methyl methacrylate)," *Nanotechnology*, vol. 23, no. 34, Article ID 344014, 7 pages, 2012.

[14] D. I. Son, D. H. Park, J. B. Kim et al., "Bistable organic memory device with gold nanoparticles embedded in a conducting poly(*N*-vinylcarbazole) colloids hybrid," *Journal of Physical Chemistry C*, vol. 115, no. 5, pp. 2341–2348, 2011.

[15] H.-T. Lin, Z. Pei, J.-R. Chen, G.-W. Hwang, J.-F. Fan, and Y.-J. Chan, "A new nonvolatile bistable polymer-nanoparticle memory device," *IEEE Electron Device Letters*, vol. 28, no. 11, pp. 951–953, 2007.

[16] H.-C. Chang, C.-L. Liu, and W.-C. Chen, "Flexible nonvolatile transistor memory devices based on one-dimensional electrospun P3HT:Au hybrid nanofibers," *Advanced Functional Materials*, vol. 23, no. 39, pp. 4960–4968, 2013.

[17] A. Prakash, J. Ouyang, J.-L. Lin, and Y. Yang, "Polymer memory device based on conjugated polymer and gold nanoparticles," *Journal of Applied Physics*, vol. 100, no. 5, Article ID 054309, 2006.

[18] S. A. Ponomarenko, E. A. Tatarinova, A. M. Muzafarov et al., "Star-shaped oligothiophenes for solution-processible organic electronics: flexible aliphatic spacers approach," *Chemistry of Materials*, vol. 18, no. 17, pp. 4101–4108, 2006.

[19] I. Barlow, S. Sun, G. J. Leggett, and M. Turner, "Synthesis, monolayer formation, characterization, and nanometer-scale photolithographic patterning of conjugated oligomers bearing terminal thioacetates," *Langmuir*, vol. 26, no. 6, pp. 4449–4458, 2010.

[20] H. S. Kato, Y. Murakami, Y. Kiriyama et al., "Decay of the exciton in quaterthiophene-terminated alkanethiolate self-assembled monolayers on Au(111)," *The Journal of Physical Chemistry C*, vol. 119, no. 13, pp. 7400–7407, 2015.

[21] C. Nogues, P. Lang, M. R. Vilar et al., "SAMs functionalised by -quaterthiophene as model for polythiophene grafting," *Colloids and Surfaces A: Physicochemical and Engineering Aspects*, vol. 198–200, pp. 577–591, 2002.

[22] R. Michalitsch, A. ElKassmi, A. Yassar, and F. Garnier, "A practical synthesis of functionalized alkyl-oligothiophenes for molecular self-assembly," *Journal of Heterocyclic Chemistry*, vol. 38, no. 3, pp. 649–653, 2001.